

LASCO Measurements of the Energetics of Coronal Mass Ejections

A. Vourlidas, P. Subramanian

Center for Earth Observing and Space Research, Institute for Computational Sciences, George Mason University, Fairfax, VA 22030
avourlid@pythia.nrl.navy.mil

and

K. P. Dere, R. A. Howard

E. O. Hulbert Center for Space Research, Naval Research Laboratory, Washington, DC 20375

ABSTRACT

We examine the energetics of Coronal Mass Ejections (CMEs) with data from the LASCO coronagraphs on SOHO. The LASCO observations provide fairly direct measurements of the mass, velocity and dimensions of CMEs. Using these basic measurements, we determine the potential and kinetic energies and their evolution for several CMEs that exhibit a flux-rope morphology. Assuming flux conservation, we use observations of the magnetic flux in a variety of magnetic clouds near the Earth to determine the magnetic flux and magnetic energy in CMEs near the Sun. We find that the potential and kinetic energies increase at the expense of the magnetic energy as the CME moves out, keeping the total energy roughly constant. This demonstrates that flux rope CMEs are magnetically driven. Furthermore, since their total energy is constant, the flux rope parts of the CMEs can be considered to be a closed system above $\sim 2 R_\odot$.

Subject headings: Sun: activity — Sun: corona — Sun: magnetic fields — Sun: solar-terrestrial relations

1. Introduction

Material ejections are a common phenomenon of the solar corona. Since the first observation on 14 December 1971 (Tousey 1973), several thousands of CMEs have been seen (Howard et al. 1985; Kahler 1992; Webb 1992; Hundhausen 1997; Gosling 1997). Nevertheless, the mechanisms that cause a CME and the forces acting on it during its subsequent propagation through the corona are largely unknown. Of these two issues, the issue of CME propagation through the corona is by far more amenable. Past observations have provided insufficient coverage of the CME development for several reasons: restricted field of view of the coronagraphs, frequent orbital nights and low sensitivity of the instruments. Consequently, past studies were largely focused on either the phenomeno-

logical description and classification of CMEs or the measurement of average values for the physical properties of the events such as speed, mass, kinetic energy (Jackson and Hildner 1978; Howard et al. 1985). The study of the CME energetics, in particular, was necessarily restricted to a handful of well observed events (Rust et al. 1980; Webb et al. 1980). Their analysis revealed the importance of the (elusive) magnetic energy and established that the potential energy dominates the kinetic energy. It was also found that the energy residing in shocks, radio continua and other forms of radiation was insignificant in comparison to the mechanical energy of the ejected material.

The lessons learned from the past resulted in a greatly improved set of instruments; the LASCO coronagraphs (Brueckner et al. 1995), aboard the SOHO spacecraft (Domingo et al 1995). The loca-

tion of the spacecraft at the L1 point permits the continuous monitoring of the Sun while the combination of the three LASCO coronagraphs provides an unprecedented field of view from $1.1 R_{\odot}$ to $30 R_{\odot}$. The replacement of videcons with CCD detectors and the very low stray light levels of the coronagraphs have led to a vast sensitivity improvement. It is now possible to routinely follow the dynamical evolution of a CME. Here, we compute basic quantities; mass, velocity and geometry and derive quantities such as the potential, kinetic and magnetic energies of CMEs as they progress through the outer corona into the heliosphere. To our knowledge, this is the first time that detailed observations of the dynamical evolution of these quantities has been presented. These measurements are expected to provide concrete observationally-based constraints on the driving forces in CME models. For this study, we focus on a group of CMEs that share a common characteristic; namely, they resemble a helical flux rope in the C2 and C3 coronagraph images. We choose these events for three reasons: (i) the area of a CME that corresponds to the flux rope is usually easily identifiable in the coronagraph images, (ii) their appearance can be related to the flux rope structures measured in-situ from Earth-orbiting spacecraft, and (iii) there has been extensive theoretical and observational interest for this class of CMEs.

Several CMEs observed with the LASCO instrument exhibit a helical structure like that of a flux rope (Chen et al. 1997; Dere et al. 1999; Wood et al. 1999). The theoretical basis for flux rope configurations in solar and interplanetary plasmas is well established (e.g., Gold 1963; Goldstein 1983; Chen and Garren 1993; Low 1996; Kumar and Rust 1996; Guo et al. 1996; Wu, Guo & Dryer 1997). These treatments envisage the helical flux rope as a magnetic structure that resides in the lower corona and erupts to form a CME. There is some debate about whether the flux rope is formed before the eruption, or whether it is formed as a consequence of reconnection processes that lead to the eruption. These arguments are related to those which consider whether the reconnection occurs above the sheared arcade which presumably forms the flux rope, or below it (Antiochos, Devore and Klimchuk 1999).

Neither the physical mechanisms of the initial

driving impulse, nor the conditions in the corona which determine the subsequent propagation of the flux rope are very well known from observations. Theoretical models often rely on educated guesses to model both the initiation of the CME as well as its propagation through the corona. Statements about the energetics, or driving forces behind CMEs are made on these bases; for instance, Chen (1996) and Wu et al. (1997) show plots of the variation of kinetic, potential and magnetic energies of CMEs as calculated from their models. The measurements we present in this paper are expected to yield some clues about the validity of the assumptions made in these models. It may be emphasized that our measurements are made only in the outer corona ($2.5 R_{\odot}$ - $30 R_{\odot}$). They are therefore not expected to shed much light on the energetics of the flux rope CMEs immediately following initiation, or on the initiation process itself.

Our estimates of the magnetic energy of flux-rope CMEs are made on the basis of in-situ measurements of magnetic clouds near the earth. This is because flux-rope CMEs ejected from the Sun are often expected to evolve into magnetic clouds (Rust and Kumar 1994; Kumar and Rust 1996; Chen et al. 1997; Gopalswamy et al. 1998). Conversely, in-situ measurements of magnetic clouds near the earth suggest that their magnetic field configuration resembles a flux rope (Burlaga 1988; Lepping, Jones, & Burlaga 1990; Farrugia et al. 1995; Marubashi 1997). Radio observations of moving Type-IV bursts can also probe the magnetic field in CMEs (Stewart 1985; Rust et al. 1980) but they are so rare that near-Earth measurements are the most reliable estimates of the magnetic flux. It should be borne in mind, however, that the precise relationship between CMEs and magnetic clouds and the manner in which CMEs evolve into magnetic clouds is not very well understood (Dryer 1996; Gopalswamy et al. 1998). The main reason for this situation is the simple observational fact that while CMEs are best observed off the solar limb, magnetic clouds are measured near the Earth. This issue will hopefully be addressed in the near future by the next generation of space-borne instruments.

The rest of the paper is organized as follows: We describe our methods of measuring the mass and position of a CME and of calculating the different forms of energy associated with it in § 2. § 3

presents the results of our measurements. We discuss caveats that accompany these results in § 4 and draw conclusions in § 5.

2. Data Analysis

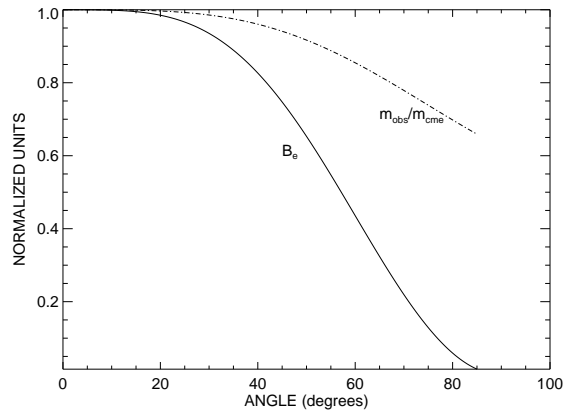


Fig. 2.— *Solid line:* Thomson scattering calculation of the angular dependence of the total brightness of a single electron at a heliocentric distance of $10 R_{\odot}$. The curve is normalized to the brightness at 0° . *Dash-dot line:* Ratio of the observed relative to the actual mass of a simulated CME, centered on the plane of the sky, as a function of its angular width (see text).

2.1. Mass calculations

White light coronagraphs detect the photospheric light scattered by the coronal electrons and therefore provide a means to measure coronal density. Transient phenomena, such as CMEs, appear as intensity (hence, density) enhancements in a sequence of coronagraph images. We compute the mass for a CME in a manner similar to that described by Poland et al. (1981). After the coronagraph images are calibrated in units of solar brightness, a suitable pre-event image is subtracted from the frames containing the CME. The excess number of electrons is simply the ratio of the excess observed brightness, B_{obs} , over the brightness, $B_e(\theta)$, of a single electron at some angle, θ , (usually assumed to be 0) from the plane of the sky. $B_e(\theta)$ is computed from the Thomson scattering function (Billings 1966). The mass, m ,

is then calculated assuming that the ejected material comprises a mix of completely ionized hydrogen and 10% helium. Namely,

$$m = \frac{B_{obs}}{B_e(\theta)} \cdot 1.97 \times 10^{-24} \text{ gr} \quad (1)$$

After the mass image is obtained, we delineate the flux rope by visual inspection, as shown in Figure 1. We attempt to circumscribe the cross section of the helical flux rope as seen in the plane of the sky. The cavity seen in the white light/mass images is taken to be the interior of the flux rope, bounded by the helical magnetic field (Figure 1). The mass contained in the flux rope is computed by summing the masses in the pixels encompassed by the flux rope.

The accuracy of the mass calculations depends on three factors: the CME depth and density distribution along the line of sight and the angular distance of the CME from the plane of the sky. All three factors are unknown since the white light observations represent only the projection of the CME on the plane of the sky. Some additional information can be obtained from pB measurements, but these are only occasionally available. Therefore, to convert the observed brightness to a mass measurement we have to make an assumption. Namely, we assume that all the mass in the CME is concentrated in the plane of the sky. Since CMEs are three-dimensional structures, our calculations will tend to underestimate the actual mass.

To quantify the errors arising from our assumption, we performed two brightness calculations shown in Figure 2. The solid line shows the angular dependence of the quantity $B_e(\theta)$ in equation (1) normalized to its value at 0° . We see that our assumption that the ejected mass is always in the sky plane ($\theta = 0^\circ$) underestimates the mass by about a factor of 2 at angles $\sim 50 - 60^\circ$. We expect that the CMEs in our sample are relatively close to the plane of the sky ($\theta < 50^\circ$) since their flux rope morphology is clearly visible.

Next, we investigate the effect of the finite width of a CME. We simulate a CME with constant density per angular bin along the line of sight, centered in the plane of the sky at a heliocentric distance of $10 R_{\odot}$. Using equation (1) we calculate the observed mass, m_{obs} , for various widths and compare it to the actual mass, m_{cme} for the same widths. The dashed line in Figure 2

shows the dependence of this ratio, m_{obs}/m_{cme} on the width of the CME. For angular widths similar to those of the CMEs in our sample ($\lesssim 60^\circ$) the mass would be underestimated by about $\sim 15\%$.

Finally, we estimate the noise in the LASCO mass images from histograms of empty sky regions. The statistics in these areas show a gaussian distribution centered at zero, as expected. We define the noise level as one standard deviation or about 5×10^8 gr in the C2 frames and 3×10^{10} gr in the C3 frames. The average C2 pixel signal in the measured CMEs is 10 times the noise and the C2 pixel signal-to-noise ratio in the mass measurements is between 10-100. The CMEs get fainter as they propagate farther from the sun. Therefore, the pixel signal-to-noise ratio in the C3 images drops to about 3-4. These figures refer to single pixel statistics and demonstrate the quality of the LASCO coronagraphs. Our measurements are based on statistics of hundreds or thousands of pixels for each image. Therefore, the “mass” noise in our images is insignificant compared to the systematic errors involved in the calculation of a CME mass as discussed previously.

In summary, these calculations suggest that the LASCO measurements tend to underestimate the CME mass by about 50%, for realistic widths and propagation angles. A more detailed analysis of CME mass calculations will appear elsewhere.

2.2. CME Energy calculations

In this analysis we consider only three forms of energy — potential, kinetic, and magnetic energy. These energies can be estimated from quantities measured directly in the LASCO images like CME area, mass and speed. Two of the many other forms of energy that can exist in the CME/corona system can be estimated based on some assumptions and educated guesses: the CME enthalpy U and the thermal energy E_T . We will show in § 4 that the thermal energy E_T is insignificant. There are several uncertainties involved in calculating the enthalpy of a CME. Firstly, the temperature structure of a CME is far from known. It is conceivable that it is composed of multithermal material. In situ measurements of magnetic clouds near the earth reveal a temperature range of $10^4 - 10^5$ K. Furthermore, it is not clear if the gas in the CMEs in the outer corona is in local thermodynamic equilibrium. Nonetheless, if we

assume the CME to be a perfect gas in local thermodynamic equilibrium with equal electron and ion temperatures, the enthalpy U can be as large as $5E_T = 5nkT$. If we assume a temperature of a million degrees K and a mass of 10^{15} gr, this yields $U \approx 3 \times 10^{29}$ ergs. As will be seen later, even this upper limit for the enthalpy U is lower than the kinetic and potential energies by at least one order of magnitude, except in the lower corona where it can be comparable to the kinetic energy. Furthermore, the enthalpy is directly proportional to the mass, which, as will be seen later, remains approximately constant as the CME propagates outwards. We therefore conclude that the enthalpy is a small, constant magnitude correction which can be safely neglected without affecting the overall conclusions regarding CME energetics.

Potential Energy We define the potential energy of the flux rope as the amount of energy required to lift its mass from the solar surface. The gravitational potential energy is calculated using

$$E_P = \sum_{\text{flux rope}} \int_{R_\odot}^R \frac{GM_\odot m_i}{r_i^2} dr_i, \quad (2)$$

where m_i and r_i denote the mass and distance from sun-center respectively, of each pixel, M_\odot is the mass of the sun, R_\odot is the solar radius and G is the gravitational constant. The summation is taken over the pixels comprising the flux rope (Figure 1).

Kinetic Energy We use the center of mass of the flux rope to describe its movement. The location of the center of mass relative to the sun center is given by

$$\vec{r}_{CM} = \frac{\sum_{\text{flux rope}} m_i \vec{r}_i}{\sum_{\text{flux rope}} m_i}, \quad (3)$$

where \vec{r}_{CM} is the radius vector of the center of mass and \vec{r}_i is the radius vector for each pixel. The summation, as before, is taken over the pixels comprising the flux rope. We calculate \vec{r}_{CM} for each CME frame as it progresses through the LASCO field of view. In other words, we compile a table of center-of-mass locations versus time, (\vec{r}_{CM}, t) . By fitting a second degree polynomial to (\vec{r}_{CM}, t)

we obtain the center of mass velocity, \vec{v}_{CM} and acceleration \vec{a}_{CM} . The calculation of the speed and acceleration as described above has the advantage of involving only the measurement of the CME center of mass. Once the flux rope is delineated, its mass, speed and energetics follow. The kinetic energy is simply

$$E_K = \frac{1}{2} \sum_{\text{flux rope}} m_i v_{CM}^2. \quad (4)$$

Note that these measurements are based on the plane of the sky location of the center of mass. The speed used in the calculations is therefore a projected quantity and not the true radial speed. It follows that the derived kinetic energies are lower limits. The same applies for all of our observed and derived quantities which facilitates the comparison among the different events.

Magnetic Energy The calculations of the potential and kinetic energies of flux rope CMEs are made directly from the mass images. On the other hand, the values we use for the magnetic energy of these CMEs are only estimates because the magnetic field strength in a CME is unknown. In-situ measurements by spacecraft like WIND yield the magnetic field contained in magnetic clouds observed near the earth. As mentioned in § 1, helical flux-rope CMEs are thought to evolve into magnetic clouds similar to those observed at the earth. Therefore, measurements of the magnetic flux contained in such magnetic clouds are expected to be fairly representative of that carried by flux rope CMEs. The magnetic energy carried by a flux rope CME is defined by

$$E_M = \frac{1}{8\pi} \int_{\text{flux rope}} B^2 dV, \quad (5)$$

where B is the magnetic field carried by the flux rope, and the integration is carried out over the volume of the flux rope. For a highly conducting medium such as the heliosphere, the magnetic flux, $\int B dA$, is frozen into the CME as it evolves to form a magnetic cloud. The magnetic flux measured in-situ is therefore taken to be the same as that contained in the CME as it passes through the LASCO field of view. We use this frozen flux assumption since we feel that it is a simple, physically motivated one. Another assumption which

gives very similar results is conservation of magnetic helicity (Kumar and Rust 1996). The volume integral in equation (5) contains another unknown; the volume occupied by the flux rope. Assuming a cylindrical flux rope with constant magnetic field, equation (5) is approximated as

$$E_M \sim \frac{1}{8\pi} \frac{l}{A} (B \cdot A)^2, \quad (6)$$

where A is the area of flux rope as measured in the LASCO images and l is the length of flux rope. The quantity $B \cdot A$ is the magnetic flux frozen into the flux rope and is conserved. For our purposes, we need, in equation (6), a representative value for the magnetic flux of a flux rope. We obtain such an estimate from model fits (Lepping, Jones, & Burlaga 1990) to several magnetic clouds observed by WIND between 1995–1998 available at http://lepmf.gsfc.nasa.gov/mfi/mag_cloud_pub1p.html. We only consider clouds that occurred at the same time interval as the LASCO CMEs (1997–98). From this sample we get the average magnetic flux, $\langle B \cdot A \rangle = 1.3 \pm 1.1 \times 10^{21} \text{ G cm}^2$ which we put in equation (6). The resulting magnetic energy uncertainty is then $(1.1/1.3)^2 \approx 70\%$. To calculate the magnetic energy, we also need the length l of the rope along the line of sight. Since the true length of the rope cannot be obtained observationally, we assume that the flux rope is expanding in a self-similar manner, with its length being proportional to its heliocentric height; namely, $l \sim r_{CM}$.

Finally, we emphasize that the magnetic cloud data used here are only representative. They are not measurements from the same LASCO events we analyzed. Also the magnetic flux in individual events can differ from the average value we adopted. Furthermore, the magnetic field values we use refer to the total (toroidal + poloidal) magnetic field contained in the flux rope. The definition of $B \cdot A$, however, refers only to the toroidal component of the magnetic field which is normal to the cross-sectional area of the flux rope. For these reasons, it is difficult to ascribe errors to our magnetic energy calculations of individual events. Therefore, we decided to use the statistical uncertainty in the average flux to compute the error in the magnetic energy which is about 70% as shown above. It is unfortunate that the magnetic energy measurements are so uncertain and they will

TABLE 1
CME EVENT LIST

Date	First C2 appearance (UT)	Position angle CCW from North (Deg)	Angular Width (Deg)	Final Speed (km/sec)
970223 ^{ab}	02:55	89	63	920
970413 ^c	16:12	260	42	520
970430 ^a	04:50	83	70	330
970813 ^d	08:26	272	36	350
971019 ^b	04:42	90	77	263
971030	18:21 ^f	85	50	215
971031	09:30	260	54	476
981101 ^b	20:11	272	57	264
980204	17:02	284	43	420
980224	07:55	88	32	490
980602 ^e	09:37	246	47	600

^aWood et al. (1999)

^bDere et al. (1999)

^cChen et al. (1997)

^dAndrews and Howard (1999)

^ePlunkett, Vourlidas, & Simberova (2000)

^fThe time refers to the previous day, 97/10/29.

continue to be so until direct observations of the coronal magnetic field become available.

3. Results

For our analysis, we searched the LASCO database for CMEs with clear flux rope morphologies. We picked 11 events for which we compiled the evolution of the mass and velocity of the center of mass and the potential, kinetic and magnetic energies as the CME progressed through the LASCO C2 and C3 fields of view. For reference purposes we present a list of the events in Table 1. The information for the 1997 CMEs is taken from the LASCO CME list compiled by Chris St. Cyr (<http://lasco-www.nrl.navy.mil/cmelist.html>) except for the final speeds in the last column that refer to the center of mass of the fluxropes and were calculated by us. Further information on source regions and associated photospheric/low corona emissions for some of these events can be found in the references noted in the table.

Our measurements are shown in Figures 3 – 6. The horizontal axis denotes heliocentric height in solar radii. Each row is a separate CME event, labeled by its date of observation by the LASCO/C2 coronagraph. The left panels show the evolution of the potential, kinetic, magnetic and total energy in the CME. The total energy is the sum of the potential, kinetic and magnetic energies. The right panels show the evolution of the flux rope mass and the center-of-mass speed. As discussed in § 2, a second degree fit to (\vec{r}_{CM}, t) yields the acceleration of the center of mass \vec{a}_{CM} . The radial component of \vec{a}_{CM} is also shown in this panel. The dash-dot line, visible in some plots, marks the escape speed from the Sun as a function of height.

An inspection of the plots leads to the following overall conclusions that hold for most of the events:

- The total energy (curves marked with +) is relatively constant, to within a factor of 2, for the majority of the events despite the substantial variation seen in the individual energies. This suggests that, for radii between approximately $3R_{\odot}$ and $30R_{\odot}$, the flux rope part of these CMEs can be considered as an isolated system; i.e., there is no additional “driving energy” other than

the energies we have already taken into account (potential and kinetic energies of the flux rope, and magnetic energy associated with the magnetic field inside the flux rope).

- We see that the kinetic and, (to a lesser degree) potential energies increase at the expense of the magnetic energy, keeping the total energy fairly constant. The decrease in magnetic energy is a direct consequence of the expansion of the CME. It could imply that the untwisting of the flux rope might be providing the necessary energy for the outward propagation of the CME in a steady-state situation.
- The center of mass accelerates for most of the events, and the CMEs achieve escape velocity at heights of around $8-10 R_{\odot}$, well within the LASCO/C3 field of view.
- The mass in the flux rope remains fairly constant for some events (e.g., 97/08/13 or 97/10/30) while other events (e.g., 97/11/01 or 98/02/04) exhibit a significant mass increase in lower heights and tend to a constant value in the outer corona, above about $10-15 R_{\odot}$. This observation raises the question: why is pile up of preexisting material observed only in some flux rope CMEs? We plan to investigate this effect further in the future. It would also be interesting to examine how the mass increase close to the Sun relates to interplanetary “snowplowing” observations (Webb, Howard, & Jackson 1996).

The only notable exception is the event of 98/06/02 which is also the most massive and its total energy increases with distance from the center of the sun. This CME is associated with an exceptionally bright prominence which may affect the measurements. A detailed analysis of this event is presented in Plunkett, Vourlidas, & Simberova (2000).

4. Discussion

The conclusions of the previous section are based on a set of broadband white light coronagraph observations. The accuracy of the measurement of any structure (i.e., CME) in such images is inherently restricted by three unknowns: the

amount and distribution of the material and the extent of the structure along the line of sight.

We addressed the first two problems in § 2 where we showed that for the case of a uniformly filled CME extending ± 80 degrees out of the plane of the sky, we will measure about 65% of its mass. Since the potential and kinetic energies are directly proportional to the mass, our measurements in Figures 3 - 6 could be higher by as much as 35%. The spatial distribution of the material will also affect the visibility of the structures we are trying to measure. Because we delineate the area of the flux rope by visual inspection, we might not be following the same cross section as the structure evolves. This might account for some of the variability of the energy curves. However, we chose the CMEs based on their clear flux rope signatures. The measurements involve hundreds or even thousands of pixels per image and therefore we don't expect that the trends seen in the data are affected by the slight changes in the visibility of the structure.

The widths along the line of sight of the observed CMEs are difficult to quantify. There is no way to measure this quantity with any instrumentation in existence today. Only the magnetic energy depends on the width of the flux rope. In § 2.2, we assumed that the width of the flux rope is equal to the height of its center of mass which implies that its preeruption length is about a solar radius. Prominences and loop arcades of this length are not uncommon features on the solar surface.

As described in § 1, flux rope CMEs are expected to evolve into magnetic clouds near the earth. This is the basis on which we use in-situ data to estimate the magnetic energy carried by the flux rope CMEs (§ 2). In § 2, we also estimated that the overall normalization of the magnetic energy curve is uncertain by about 70%.

In summary, none of the above errors can affect the trends of the curves for a given event. Only the magnitudes of the various energies could change. Finally, some of the variability of the measured quantities could be attributed to the intrinsic variability of the corona and/or of the CME structure itself and cannot be removed without affecting the photometry. For this reason, it is rather difficult to associate an error estimate to individual measurements. Therefore, we decided not to include

any error bars in our figures.

The analysis of the CME dynamics in Figures 3-6 reveals an interesting trend; namely, the total energy remains constant. It appears that the flux rope part of a CME propagates as a self-contained system where the magnetic energy decrease drives the dynamical evolution of the system. All the necessary energy for the propagation of the CME must be injected in the erupting structures during the initial stages of the event. The notions that these CMEs are indeed magnetically driven and that the thermal energy contribution can be ignored are further reinforced by the magnitude of the plasma β parameter (Fig. 7). The calculations were performed with the assumption that the CME material is at a coronal temperature of 10^6 K. We see that the CMEs have a very small β (except the events on 98/02/04 and 98/06/02) which increases slightly outwards. It appears to tend towards a constant value. Such a behavior for the plasma β parameter was predicted in the flux rope model of Kumar and Rust (1996). We also find that the potential energy is larger than the kinetic energy. These results confirm the conclusions from earlier Skylab measurements (see Rust et al. (1980) for details).

The relation between the helical structures seen in the coronagraph images and eruptive prominences is still unclear. In our sample, only half of the CMEs have clear associations with eruptive prominences (e.g., 97/02/23). No helical structures are visible in pre-eruption EIT 195Å images, in agreement with past work (Dere et al. 1999). On the other hand, the flux rope of the event on 98/06/02 is very clearly located above the erupting prominence and there is strong evidence that it was formed before the eruption (Plunkett, Vourlidas, & Simberova 2000). It seems, therefore, likely that the process of the formation of the flux rope is completed during the early stages of the eruption at heights below the C2 field of view ($< 2 R_\odot$). Such an investigation, however, is beyond the scope of this paper.

Finally, we turn our attention to the evolution of the flux rope shape as a function of height. We proceed by comparing the velocity of the CME front to its center of mass velocity. Because the visual identification of points along the front can be influenced by visibility changes as the CME evolves, it is susceptible to error. A better method

is to use a statistical measure for the location of the front such as the center of mass. Hence, the location of the front is defined as the center of mass of the pixels that lie within $0.1 R_{\odot}$ of the front of the flux rope and within $\pm 25^{\circ}$ of the radial line that connects the sun center with the center of mass. The velocity of the front, v_f is calculated in the same manner as v_{CM} (§ 2.2). The comparison of the two velocity profiles for some representative events is shown in Figure 8. Six of the eleven CMEs have profiles similar to 97/08/13 (self-similar expansion) or 97/10/30 (no expansion), while five show a progressive flattening such as 97/04/13 or 97/11/01, similar to that found in Wood et al. (1999). Some theoretical flux rope models also predict flattening of the flux rope as it propagates outwards (Chen et al. 1997; Wood et al. 1999).

5. Conclusions

We have examined, for the first time, the energetics of 11 flux rope CMEs as they progress through the outer corona into the heliosphere. The kinetic and potential energies are computed directly from calibrated LASCO C2 and C3 images, while the magnetic energy is based on estimates from near-Earth in-situ measurements of magnetic clouds. These results are expected to provide constraints on flux rope models of CMEs and shed light on the mechanisms that drive such CMEs. These measurements provide no information about the initial phases of the CME (at radii below $\sim 2R_{\odot}$). All the measurements and conclusions hold for heights in the C2 and C3 fields of view; between 3 and $30R_{\odot}$. The salient conclusions from an examination of 11 CMEs with a flux rope morphology are:

- For relatively slow CMEs, which constitute the majority of events,
 - The potential energy is greater than the kinetic energy.
 - The magnetic energy advected by the flux rope is given up to the potential and kinetic energies, keeping the total energy roughly constant. In this sense, these events are magnetically driven.
- For the relatively fast CMEs with velocities ≥ 600 km/s (97/02/23, 98/06/02),

- The kinetic energy exceeds the potential energy by the time they reach the outer corona (above $\sim 15R_{\odot}$).
- The magnetic energy carried by flux rope is significantly below the potential and kinetic energies.

We thank D. Spicer for the initial discussions that led to this paper and the referee for his/her constructive comments. SOHO is an international collaboration between NASA and ESA and is part of the International Solar Terrestrial Physics Program. LASCO was constructed by a consortium of institutions: the Naval Research Laboratory (Washington, DC, USA), the University of Birmingham (Birmingham, UK), the Max-Planck-Institut für Aeronomie (Katlenburg-Lindau, Germany) and the Laboratoire d’Astronomie Spatiale (Marseille, France).

REFERENCES

Andrews, M. D., & Howard, R. A. 1999, in AIP Conf. Proc. 471, Solar Wind Nine, eds. S.R. Habbal et al. (Woodbury: AIP), 629

Antiochos, S. K., Devore, C. R., & Klimchuk, J. A. 1999, ApJ, 510, 485

Billings, D. E. 1966, a Guide to the Solar Corona, (New York: Academic Press)

Brueckner, G. E., et al. 1995, Sol. Phys., 162, 291

Burlaga, L. F. 1988, J. Geophys. Res., 93, 7217

Chen, J., & Garren, D. A. 1993, J. Geophys. Res., 20, 2319

Chen, J. 1996, J. Geophys. Res., 101, 27499

Chen, J. et al. 1997, ApJ, 490, L191

Dere, K. P. et al. 1999, ApJ, 516, 465

Domingo, V., Fleck, B., and Poland, A. I. 1995, Sol. Phys., 162, 1

Dryer M. 1996, Sol. Phys., 169, 421

Farrugia, C. J., Osherovich, V. A., and Burlaga, L. F., 1995, J. Geophys. Res., 100, 12293

Gold, T. 1963, Proc. Pontifical Acad. of Sciences, Vatican 25, 431

Goldstein, H. 1983, in NASA Conf. Publ. 2280, Solar Wind Five, ed. M. Neugebauer, NASA CP-2280, 731

Gopalswamy, N. et al. 1998, *Geophys. Res. Lett.*, 25, 2485

Gosling, J. T. 1997, in AGU Geophys. Monograph 99, Coronal Mass Ejections, ed. N. Crooker, J. A. Joselyn & J. Feynman (Washington, D.C.: AGU), 9

Guo, W. P., Wu, S. T., & Tandberg-Hanssen, E., 1996, *ApJ*, 469, 944

Howard, R. A., Sheeley, N. R., Koomen, M., J., Michels, D. J. 1985, *J. Geophys. Res.*, 90, 8173

Hundhausen, A. G. 1997, in *Cosmic Winds and the Heliosphere*, eds. J. R. Jokipii, C. P. Sonett, & M. S. Giampapa (Tucson: Univ. of Arizona Press)

Jackson, B. V., & Hildner, E. 1978, *Sol. Phys.*, 60, 155

Kahler, S. 1992, *ARA&A*, 30, 113

Lepping, R. P., Jones, J. A., & Burlaga, L. F. 1990, *J. Geophys. Res.*, 95, 11957

Low, B. C. 1996, *Sol. Phys.*, 167, 217

Kumar, A., & Rust, D. M. 1996, *J. Geophys. Res.*, 101, 15667

Marubashi, K. 1997, in AGU Geophys. Monograph 99, Coronal Mass Ejections, ed. N. Crooker, J. A. Joselyn & J. Feynman (Washington, D.C.: AGU), 147

Poland, A. I. et al., 1981, *Sol. Phys.*, 69, 169

Plunkett, S. P., Vourlidas, A., & Simberova, S. 2000, *Sol. Phys.*, in print

Rust, D. M. et al. 1980 in *Solar Flares: A Monograph from Skylab Solar Workshop II*, ed. P. A. Sturrock (Boulder: Colorado Univ. Press), 273

Rust, D. M., & Kumar, A. 1994, *Sol. Phys.*, 155, 69

Stewart, R. T. 1985 in *Solar Radiophysics*, eds. D. J. McLean & N. R. Labrum (Cambridge: Cambridge Univ. Press), 361

Tousey, R. 1973 in *Space Research XIII*, eds. M. J. Rycroft & S. K. Runcorn (Berlin: Akademie-Verlag), 713

Webb, D. F. et al. 1980 in *Solar Flares: A Monograph from Skylab Solar Workshop II*, ed. P. A. Sturrock (Boulder: Colorado Univ. Press), 471

Webb, D. F. 1992, in *Eruptive Solar Flares*, eds. Z. Svestka, B. V. Jackson & M. Machado (New York: Springer-Verlag), 234

Webb, D. F., Howard, R. A., & Jackson, B. V. 1996, in *Proceedings of the Eighth Solar Wind Conf.*, ed. D. Winterhalter et al. (New York: AIP), 540

Wood, B. E. et al. 1999, *ApJ*, 512, 484

Wu, S. T., Guo, W. P., & Dryer, M., 1997, *Sol. Phys.*, 170, 265

Wu, S. T. et al. 1997, *Sol. Phys.*, 175, 719

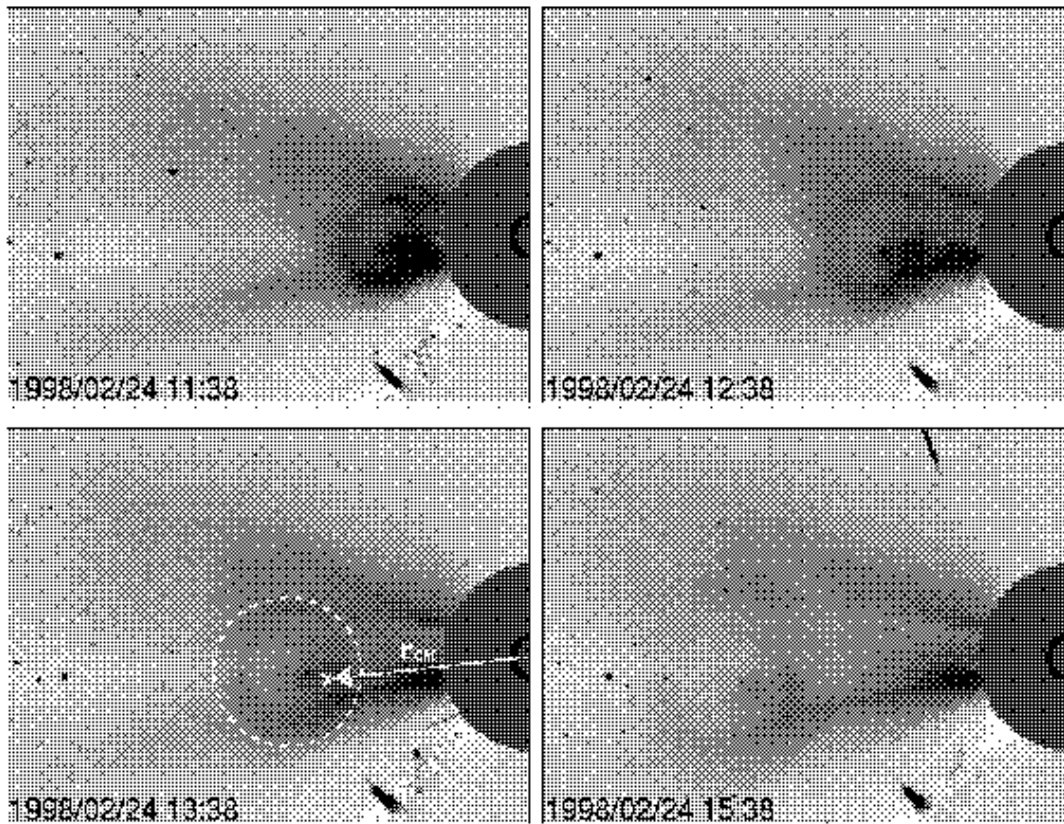


Fig. 1.— A typical flux-rope CME seen at the eastern half of the LASCO/C3 coronagraph. The small black circle inside the occulter represents the solar disk. The helical structure reminiscent of a flux rope projected on the plane of the sky is easily discernible. The dashed circle in the lower left panel demarcates the flux rope part of the CME used in our calculations. The location of the center of mass is marked with an 'x' and its vector is r_{CM} .

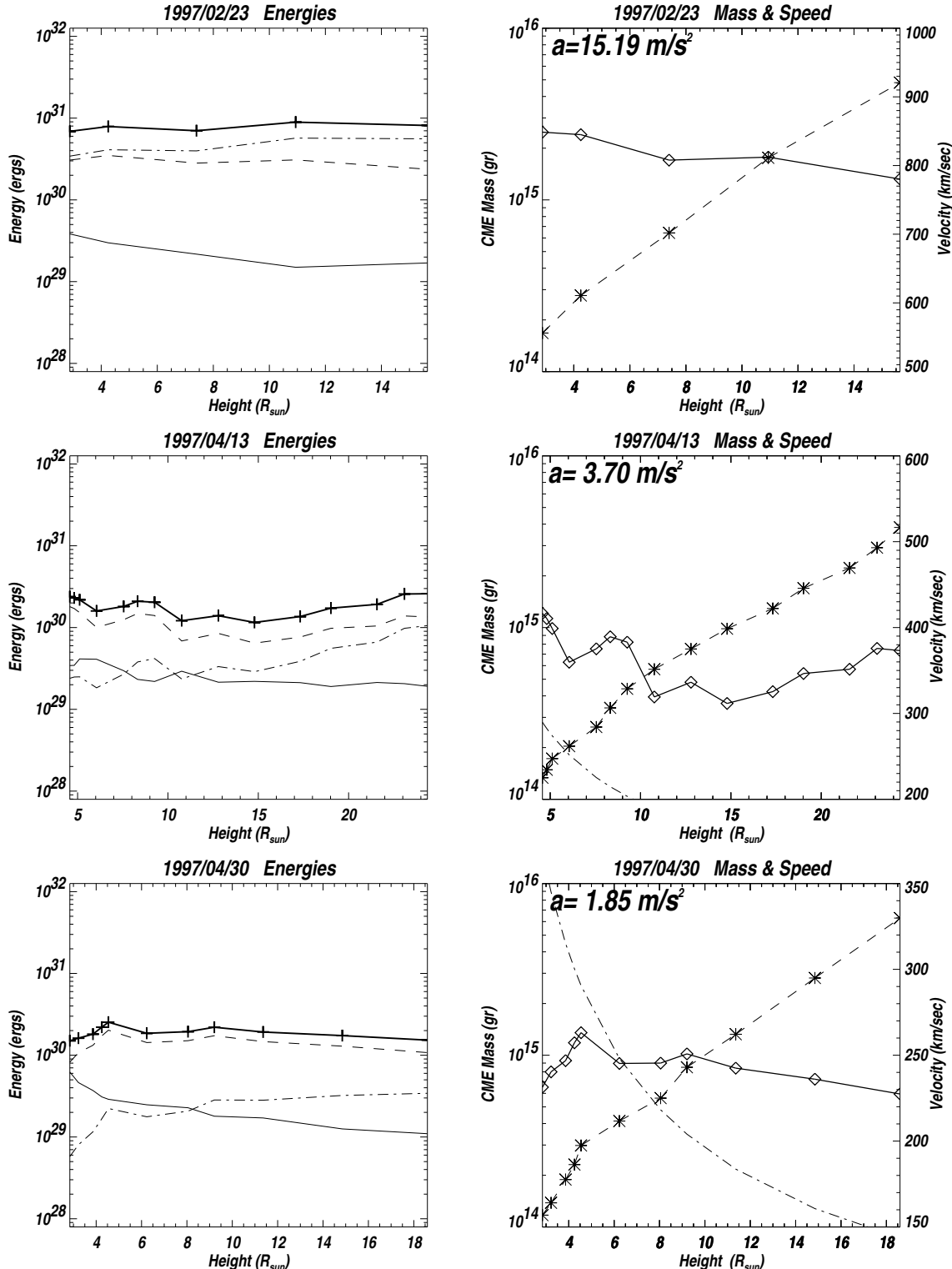


Fig. 3.— LASCO measurements of CMEs. Each row is a separate event, labeled by its observation date in the C2 coronagraph. The horizontal axis denotes heliocentric height (in R_{\odot}). *Left panels:* Evolution of potential (dash), kinetic (dash-dot), magnetic (solid) and total (solid with pluses) CME energies. The total energy is the sum of the potential, kinetic and magnetic energies. *Right panels:* Evolution of the mass (solid line with diamonds) and the center-of-mass speed (dashed line with asterisks). The derived acceleration is also shown. The dash-dot line, visible in some plots, is the escape speed from the Sun as a function of height.

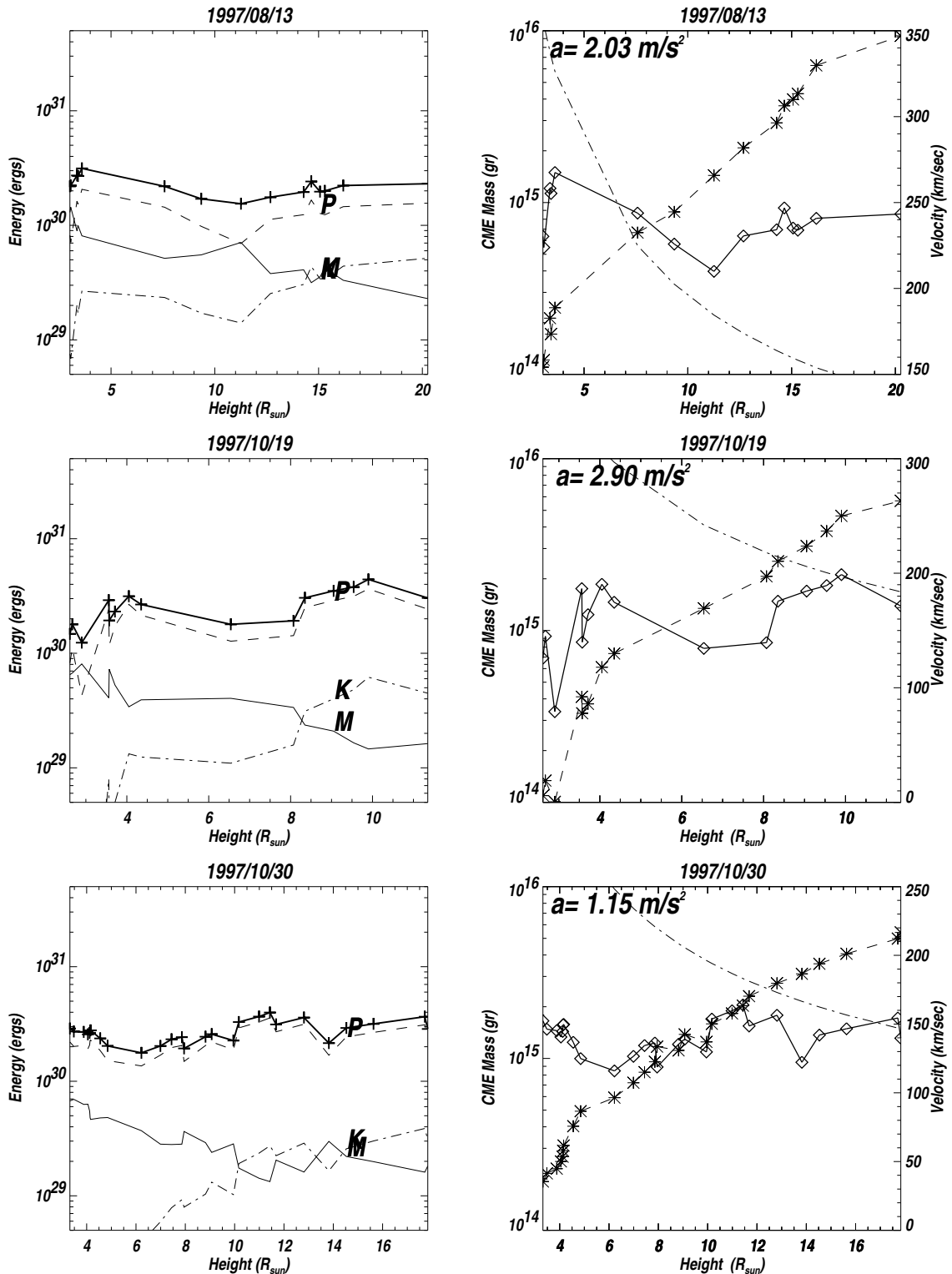


Fig. 4.— Same as Figure 3.

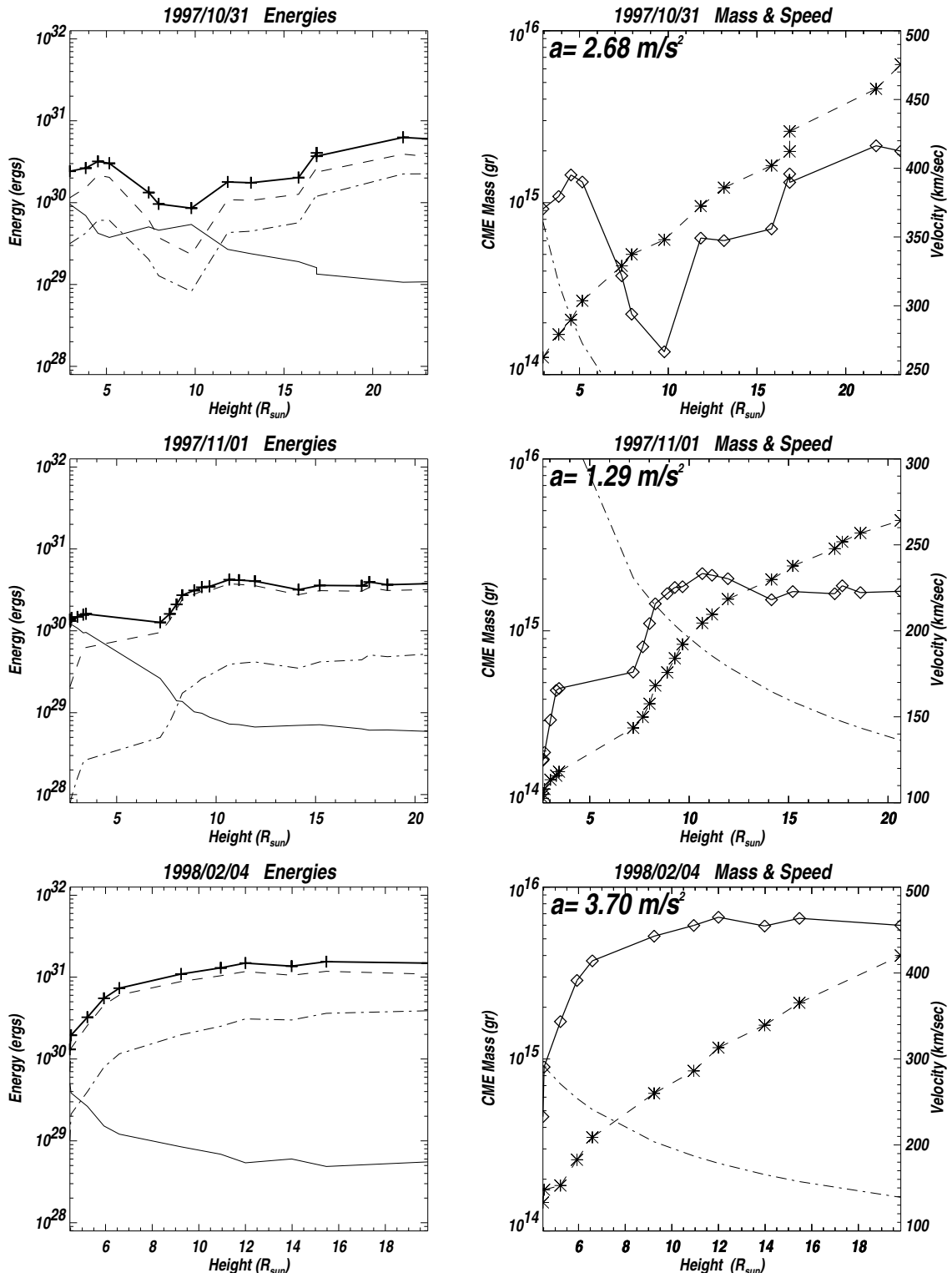


Fig. 5.— Same as Figure 3.

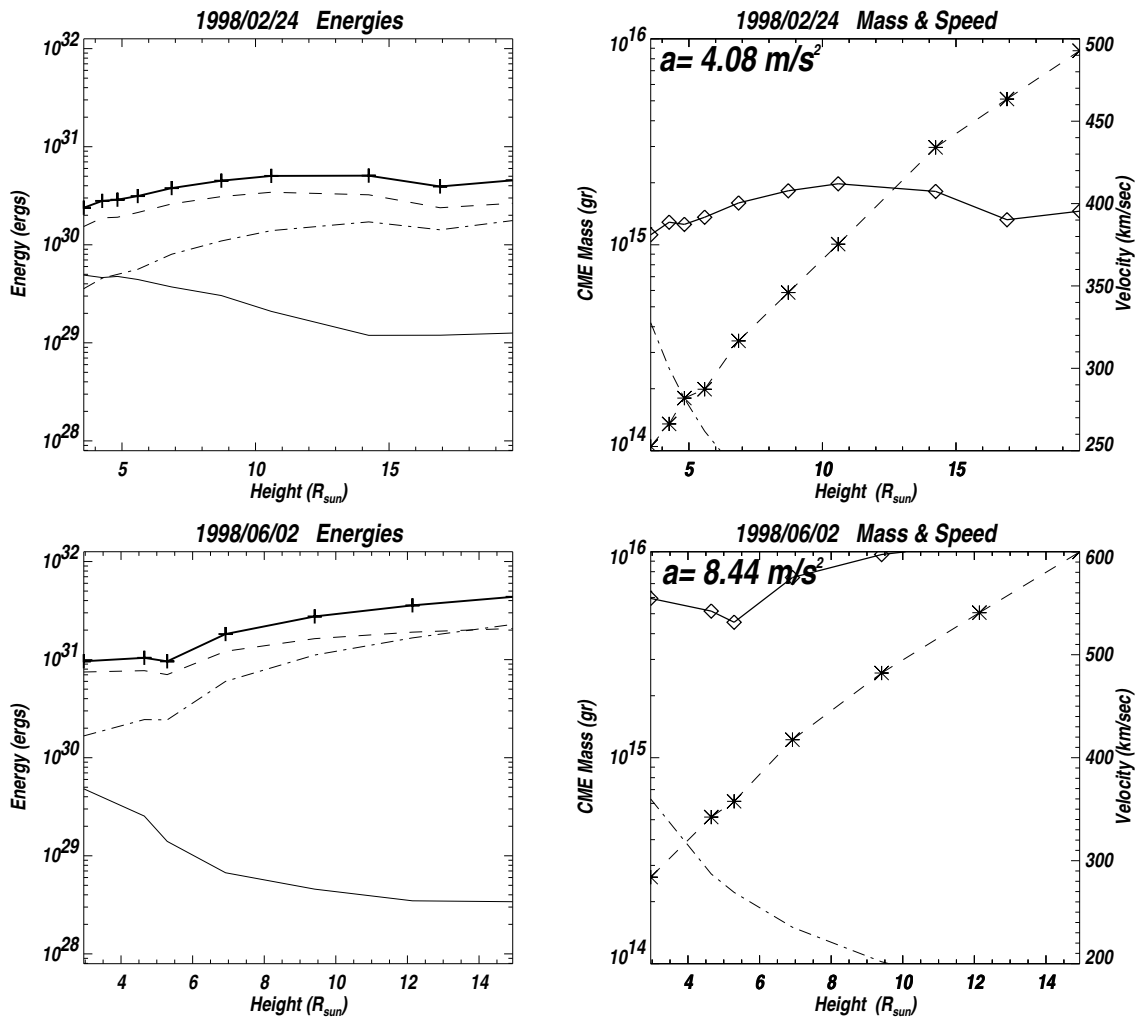


Fig. 6.— Same as Figure 3.

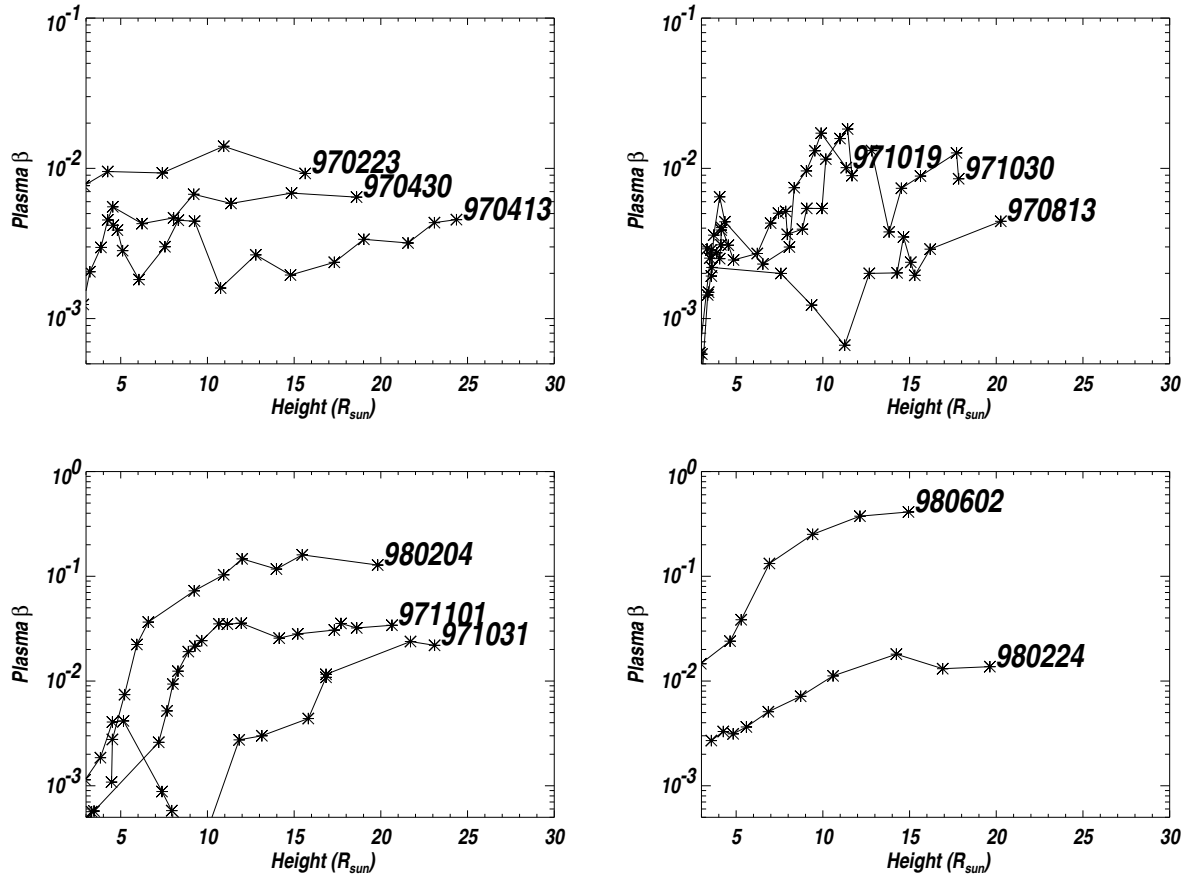


Fig. 7.— Plot of plasma β as a function of height for the flux rope CMEs. We assumed that the CME material is at a temperature of 10^6 K.

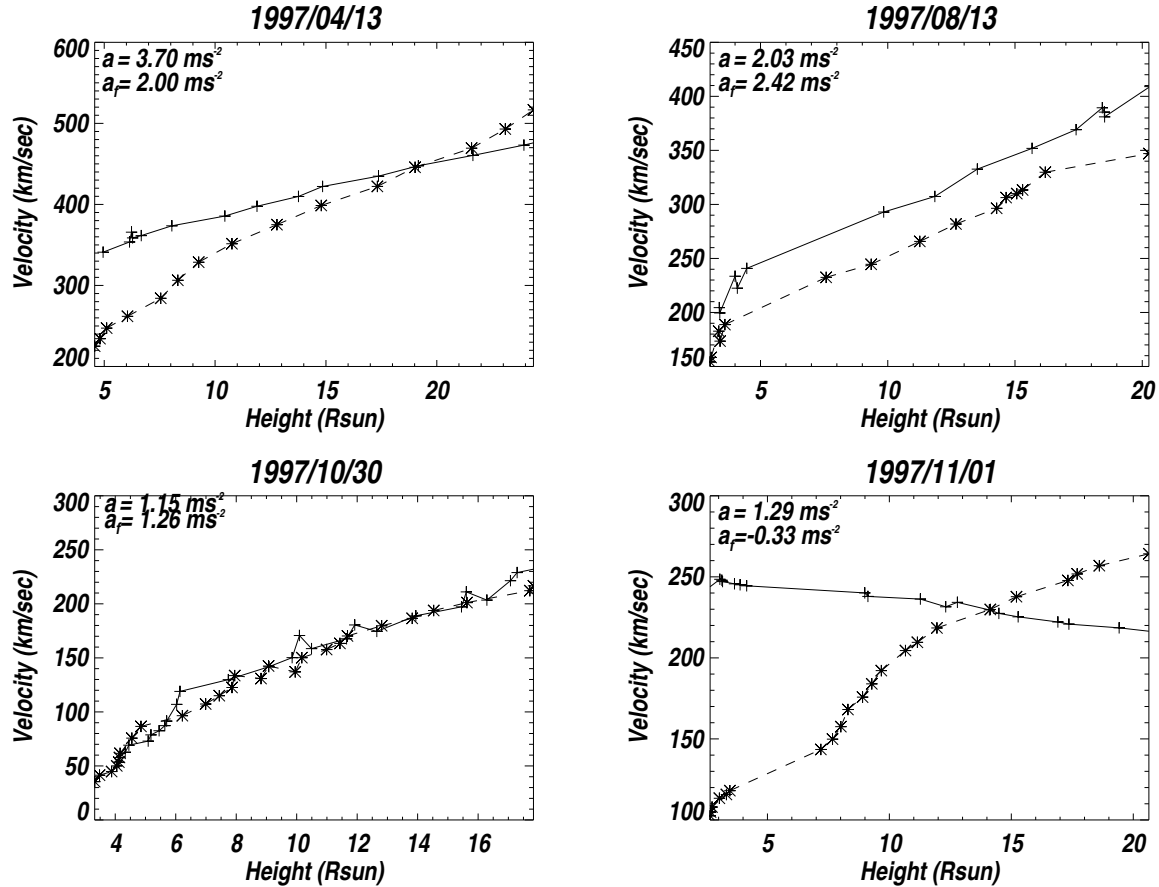


Fig. 8.— Comparison of the speeds between the front (crosses) and the center of mass (asterisks) of the flux rope for four representative events. The acceleration resulting for a polynomial fit to these curves is also shown where a and a_f are the acceleration of the center of mass and the front, respectively.